Measurement of phonon lifetimes in bulk superconducting tin

B. Pannetier and J. P. Maneval
*Groupe de Physique des Solides de l'Ecole Normale Supérieure,**
24 rue Lhomond, 75231 Paris 05, France
(Received 24 April 1980)

Phonon transport in β-Sn crystals was studied by heat-pulse techniques using superconducting tunnel junctions as detectors. At low temperature (0.6 K), pure ballistic propagation was observed up to the frequency cutoff (~ 280 GHz) set by the pair-breaking processes; hence, we could determine the (anisotropic) superconducting gap associated with a given phonon mode. Then, the temperature-dependent attenuation by thermal quasiparticles was measured at fixed frequencies $\gtrsim 150$ GHz. For that particular experiment, the sensitivity of the Al detector was calibrated against a known optical flux. Extrapolation of the attenuation coefficients to the gap frequency leads to pair-breaking mean free paths in tin ranging from 1300 Å for the slow transverse mode with wave vector along [110], to 6700 Å for the longitudinal mode along [001]; this is much in excess of estimates from thin-film experiments quoted in the literature.

I. INTRODUCTION

Electron-phonon interactions are known to govern the transport properties of pure metals, either in the normal or the superconducting state. More specifically, such systems as the superconducting tunnel junctions (STJ) used as phonon transducers,[1] or the superconducting films driven out of equilibrium[2] explicitly involve in their description the behavior of the coupled quasiparticle and phonon populations, the major role belonging to excitations whose energy is of the order of the superconducting gap 2Δ (typically 1 meV). Despite this importance, knowledge about high-frequency phonons remains far behind the science gathered on the electron system.

Because ultrasonic methods fail to reach the frequency range of 10^{11} to 10^{12} Hz, investigation of phonon lifetimes has had to rely upon less versatile methods, which we mention briefly now. The phonon-assisted tunnel conductance of metal-insulator-metal diodes[3] is a measure of $\alpha^2(\nu)F(\nu)$, where $\alpha^2(\nu)$ is a coupling parameter and $F(\nu)$ is the phonon density of states at the frequency ν. While useful near the Debye frequency, this method is not accurate enough in the "thermal" energy range delimited above. Besides this, Shapiro *et al.*[4] have demonstrated the adequacy of inelastic neutron scattering to determine phonon lifetimes, provided these are very short, as it occurs at 2Δ in high-gap materials. In view of these limitations, heat conductivity data, although they yield only averages over the whole phonon population, are still sought. Unfortunately, the lattice part in heat transport is in most cases not easy to separate from the electronic contribution. The same problems arise in the thin-film determinations of pair-breaking lifetimes performed on Al (Ref. 5) and Sn.[6,7] The heat-pulse method, applied recently to bulk superconductors,[8,9] to a large extent circumvents the above difficulties: (i) a phonon mode (wave vector $\vec{q}$; polarization $\vec{e}_q$) is selected by geometry plus time-of-flight analysis; (ii) phonon transport is clearly distinguished from the electron transport. Sufficient crystalline quality is the only prerequisite. Maximum accuracy obtains for mean free paths of the order of the sample length, which is realized simply in a superconductor by adjustment of the thermal quasiparticle population.

In the free-electron theory, coupling of the electrons to a pure longitudinal wave can be incorporated into a deformation potential model.[10] Apart from population, and possibly, interference factors, the squared Fourier component of the interaction of a phonon of wave vector $\vec{q}$ and velocity s, has the form (with h the Planck constant, and $q = |\vec{q}|$):

$$|g(q)|^2 = \frac{hC^2}{4\pi\rho s} q \quad , \tag{1}$$

C stands for the deformation potential constant, ρ for ion mass density. This leads to a mean free path in the normal state (at the frequency $\nu = qs/2\pi$) of

$$\Lambda_N(\nu) = h^3\rho s^2/8\pi^3 m^2 C^2 \nu \quad , \tag{2}$$

where m is the electron mass. As noted by Leibowitz[11] following Pippard,[12] the treatment of transverse waves is much more complex for there exist other types of coupling, namely the "electromagnetic" interaction and the "collision drag" effect of the impurities moving with the lattice. However, none of them competes in the GHz range with the "real metals" effects due to the departure from the free-electron model. The latter are again tractable in the deformation-potential approximation, so that Eq. (2) will hold for both the longitudinal and the

transverse phonons, provided C is endowed with $\vec{q}$ and polarization dependence.

Bardeen, Rickayzen, and Tewordt,[13] using first-order perturbation theory, computed phonon relaxation rates in ideal type I superconductors. Essentially two mechanisms take place: the phonon-quasiparticle scattering, similar in character, if not in magnitude, to the interaction with the electrons in the normal state and, for phonons of energy $h\nu \geqslant 2\Delta$, the dissociation-recombination of Cooper pairs. If one calls α_N and α_S the attenuations (inverse mean free paths) in the normal and superconducting states and by α_{QP} and α_{PB} the attenuations for the quasiparticle and the pair-breaking mechanisms, respectively, one can deduce from Ref. 13

$$\alpha_S = \alpha_{QP} + \alpha_{PB} \ , \tag{3a}$$

with

$$\frac{\alpha_{QP}}{\alpha_N}(\nu, T, \Delta) = \frac{2}{h\nu}\int_{\Delta}^{\infty} \rho(E)\rho(E+h\nu)\left[1 - \frac{\Delta^2}{E(E+h\nu)}\right][f(E) - f(E+h\nu)]\,dE \ , \tag{3b}$$

$$\frac{\alpha_{PB}}{\alpha_N}(\nu, T, \Delta) = \frac{1}{h\nu}\int_{\Delta}^{h\nu-\Delta} \rho(E)\rho(h\nu-E)\left[1 + \frac{\Delta^2}{E(h\nu-E)}\right][1 - f(E) - f(h\nu-E)]\,dE \ , \tag{3c}$$

where f is the Fermi-Dirac energy distribution function, and $\rho(E) = E/(E^2-\Delta^2)^{1/2}$ is the relative quasiparticle density of states, normalized to the normal state. The first component α_{QP} has a strong temperature dependence which reflects the variations of the quasiparticle population. On the contrary, α_{PB}, which counts the pair-breaking events, has the property of being essentially a step function of the frequency. A semilog plot of α_S/α_N as a function of ν is drawn in Fig. 1 for the case of tin (critical temperature $T_c = 3.72$ K; zero temperature gap $2\Delta_0/h = 273$ GHz). It is a universal function of the variables $h\nu/\Delta$ and T/T_c. We note for later use that, at $h\nu = 2\Delta$ and $T \ll T_c$, the pair-breaking attenuation is $\frac{1}{2}\pi$ times the normal one, while quasiparticle attenuation is negligible.

However, the ideal metal is an oversimplified picture of the Sn metal. Due to extension of the Fermi surface as far as the sixth Brillouin zone,[14] and non-sphericity of the Bloch cell functions, the matrix element of the electron-phonon interaction cannot have the simple structure of Eq. (1). This in turn entails directional dependence of the phonon lifetimes, as well as of the superconducting gap $2\Delta_{\vec{k}}$, defined in principle as the condensation energy of the electron pair of opposite spins and opposite wave vectors $\vec{k}$ and $-\vec{k}$.

Provided the electronic lifetime τ_{el} is long enough ($\nu\tau_{el} >> 1$), the energy-momentum conservation between electronic states of energy $\epsilon(\vec{k})$ and $\epsilon(\vec{k}')$, related by a phonon $(\vec{q}, \vec{e}_q)$, of frequency $\nu_{\vec{q}}$, implies (modulo a reciprocal-lattice vector)

$$\vec{k} \pm \vec{q} = \vec{k}' \ , \tag{4a}$$

$$\epsilon(\vec{k}) \pm h\nu_{\vec{q}} = \epsilon(\vec{k}') \ . \tag{4b}$$

Conditions (4a) and (4b) define on each sheet of the Fermi surface two effective zones (EZ), the one for $\vec{k}$, the other for $\vec{k}'$ (Fig. 2). In multiply-connected Fermi surfaces, the two EZ might belong to distinct sheets (umklapp processes); it is not even excluded that, for a given $\vec{q}$, each sheet be associated preferentially with one or the other of the $\vec{e}_q$. Leav-

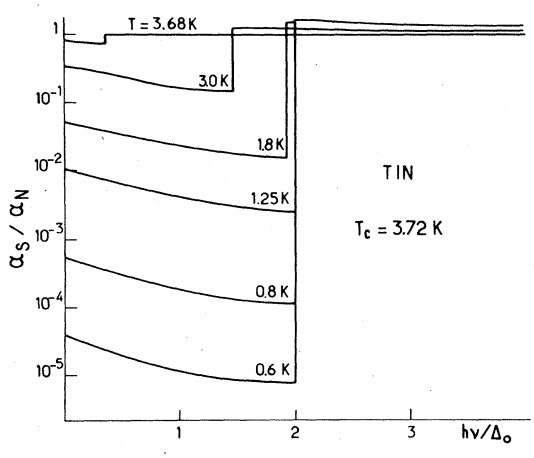

FIG. 1. Theoretical computation of the superconducting to normal attenuation ratio α_S/α_N as a function of the reduced energy parameter $h\nu/\Delta_0$, where Δ_0 is half the zero-temperature gap.

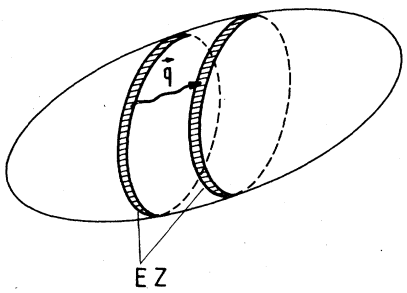

FIG. 2. Zones of the Fermi surface effective for the interaction with a phonon of wave vector $\vec{q}$ (schematic). Several sheets of the Fermi surface may participate.

ing aside these subtleties, we rather take advantage of the smallness of $\vec{q}$ to reduce the general problem. Even at the gap frequency, q is no larger than $\sim 10^7$ cm^{-1}, so that the first-order approximation in $\vec{q}$, $\vec{q}\cdot\vec{v}_k = 2\pi\nu_{\vec{q}}$ ($\vec{v}_k$ is the electronic group velocity), may be accurate enough. This is the famous "surf-riding" condition according to which the zone corresponding to a mode $(\vec{q}, \vec{e}_q)$ is practically defined by the orthogonality relation $\vec{q}\cdot\vec{v}_{\vec{k}} = 0$ (it is understood that $s \ll v_{\vec{k}}$). The superconducting attenuation is obtained through the zone integration

$$\alpha_S(\vec{q}, \vec{e}_q, T) = \frac{2}{h^2}\oint_{EZ} d\phi \frac{R_{\vec{k}}}{v_{\vec{k}}^2} |g_{\vec{k}}(\vec{q}, \vec{e}_q)|^2 \times \frac{\alpha_s}{\alpha_N}(\nu, T, \Delta_{\vec{k}}) \quad (5)$$

in which α_S/α_N is that function of ν, T, Δ, already defined by Eqs. (3a)–(3c) for the isotropic case, computed at each point $\vec{k}$ of the Fermi surface as if $\Delta = \Delta_{\vec{k}} = \text{const}$. Equation (5) results from a straightforward evaluation of the probabilities of transitions $\vec{k} \rightarrow \vec{k} \pm \vec{q}$ along the effective zone, and reduces, for longitudinal attenuation in the normal state, to Eq. (27) of Ref. 12. $R_{\vec{k}}$ is the reciprocal Gaussian curvature at point $\vec{k}$, ϕ is the angle $(0 \leq \phi < 2\pi)$ formed by the Fermi velocity with an arbitrarily fixed direction $\perp\vec{q}$ and $|g_{\vec{k}}(\vec{q}, \vec{e}_q)|^2$ is the squared matrix element introduced in Eq. (1) adapted to anisotropic electron-phonon interaction (allowing for dependences upon phonon mode and electronic state).

Thus, phonon lifetime measurements and gap measurements by phonons yield "EZ averages" specific of a given mode, instead of local values on the Fermi surface. It is not to be confused, however, with the complete smearing out of the anisotropy of, say, the phonon-measured gap which occurs when the condition $gl \gg l$ (l being the electronic mean free path) is released.[15]

In this work, one monitors the attenuation of heat pulses in the superconductor in order to get the quantities $\Lambda_N(\vec{q}, \vec{e}_q)$. To modal selection inherent in the heat-pulse method, one adds the frequency selection provided by the superconducting tunnel-junction (STJ) quantum detectors, whose threshold ν_{det} is adjustable with the gap of their constitutive material. On the other hand, low-pass filtering is set by the pair-breaking processes occurring in the bulk Sn crystal so that the "ballistic frequency window"

$$\nu_{det} \leq \nu < 2\Delta_{Sn}/h \quad (6)$$

is sorted out of the original spectrum generated in the heat pulse (Fig. 3). Our results are therefore traceable to a band, not to a single frequency, but we will see later that frequency definition is not that poor.

The paper is organized as follows: Phonon mean-free-path measured values appear in Sec. VI where they are compared to the ultrasonic, thin-film, and theoretical available data. Section II shortly describes the heat-pulse method. Material presented in Sec. III (heat-pulse velocity, anisotropy, chromatic dispersion) is an illustration of free-lattice propagation; relevant elasticity theory is summarized in the Appendix. The observations of the pair-breaking limit are presented in Sec. IV. In Sec. V finally, it is explained how the normal mean free paths are extracted from the temperature dependence of the bulk transmissivity; as the application of a STJ at varying temperature is not a usual one, we detail two independent methods of calibration we have devised for this purpose.

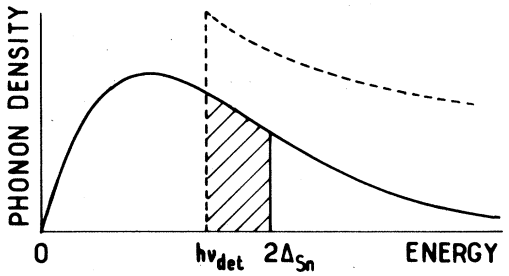

FIG. 3. Schematic of the generated phonon density spectrum (——) and detector response function (– – –) against phonon energy. $2\Delta_{Sn}$ is the mode-dependent pair-breaking limit set by the Sn crystal. Only the shaded part is detected.

II. EXPERIMENTAL TECHNIQUES

Acoustical phonons of high energy are produced in a simple fashion by heating a metallic film (copper, 350 Å) deposited by evaporation. To insulate this "phonon transducer" electrically from the propagation medium, the tin crystal is first covered with a SiO layer (5000 Å) whose quality is important as has been stressed in another context.[16] Instead of being driven by current pulses, the copper film may alternatively be excited by a laser pulse of similar duration (20 nsec) and power. For the latter case, a quarter-wavelength overlay (germanium, 320 Å) is evaporated on top of copper for more efficient photon absorption, while the copper film then has the function of thermalizing photons into acoustical phonons.

The precise shape of the emitted spectrum is of no matter in this work. However, interpretation of mean-free-path measurements becomes simpler if it can be assumed that the spectrum does not depend significantly upon the substrate (Sn) temperature T. This condition, we believe, is well satisfied in our experiments. No further than for the purpose of making an estimation, let us admit that the situation is

approximately described by the blackbody radiation model.[17] Then, the power dissipation P per unit area would be related to the heater temperature T_H by the law

$$P = \sigma(T_H^4 - T^4) \ , \tag{7}$$

where σ is the acoustic analog of the Stefan constant. It is seen that, at fixed input power, T_H and, correspondingly, the characteristic frequencies ($\nu \simeq 2.8 k_B T_H/h$ in a Planck spectrum) will be very slightly T dependent, provided $T_H >> T$ (k_B is the Boltzmann constant).

Slices with thickness from 1.0 to 4.0 mm were spark-cut from 99.999% pure single-crystal ingots (Metals Research Ltd.) along planes perpendicular to the symmetry directions [001], [110], and [100] of the tetragonal structure of white tin. Smooth rather than perfectly flat surfaces are desired since one deals with incoherent waves. To achieve this, the end faces were gently polished on a vibrating machine (Wirtz Ltd.) by using directly the thinnest grade of abrasive powder (alumina, 1 μm). The resistive electron mean free path at 4.2 K, as determined from the persistence of the Foucault inductive currents, was found to be $l \simeq 0.15$ mm.

Two materials were used in the fabrication of the superconducting tunnel junctions. Granular aluminum ($\nu_{\rm det} \simeq 150$ GHz) films (electrodes, 1000 Å each) were formed by evaporation of 99.999% pure Al out of an alumina crucible under pressure of about 2×10^{-6} torr. This method ensures reproducible critical temperature ($\simeq 2.05$ K) and energy gap ($2\Delta = 0.625$ meV) within 2%. The oxide barrier between the two electrodes was grown by allowing oxidation of the first Al film for two minutes under O_2 pressure (0.2 torr). In the case of tin junctions (2000-Å-thick electrodes), the oxidation took place at 600 torr during 16 h.

The STJ geometry was in the shape of a cross (effective area 0.2×0.2 mm^2) having a normal (4.2 K) tunnel resistance of a few 10^{-2} ohm for both the Al and the Sn junctions. Connections to the coaxial circuits were made along thin copper wires finely stuck on each electrode by means of silver painting (because the insulating SiO layer is very fragile, pressure contacts have to be discarded). Contacts are minimized so as to avoid undesirable shunt capacitances to the grounded tin sample. A couple of glass monofibers (diameter 65 μm) were installed (Fig. 4) to supply successively the emitter and the detector with the optical pulses delivered by an argon-ion laser (Spectra Physics, 4 W in continuous mode). The laser beam was initially focused into one of the fibers by means of a microscope front lens ($\times 10$) so that about 50% of the power was transmitted by the whole optical setup.

The experiments were performed in vacuum, the sample being held in thermal contact with liquid ^{3}He

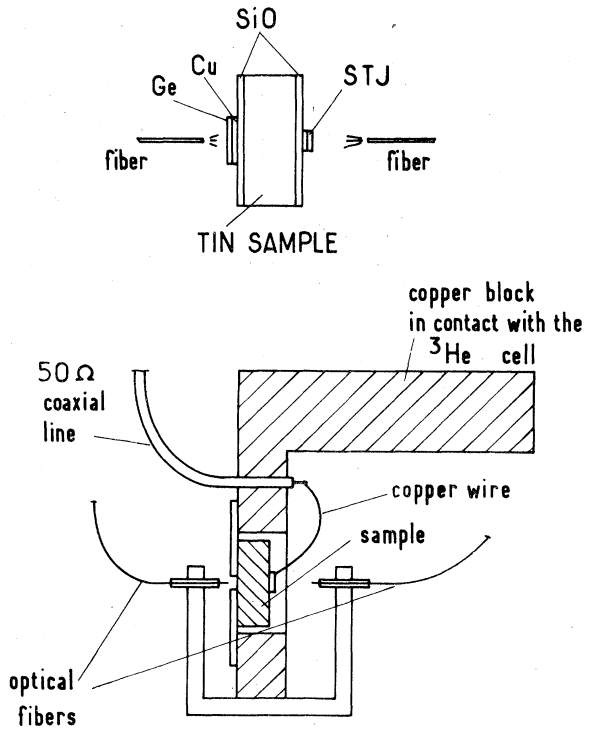

FIG. 4. Sample-holder equipped with optical and electrical feeders. Above is a representation of the thin-film transducers attached to the tin sample.

through a massive copper block. By continuous recondensing of the ^{3}He gas in the refrigerator cell, the cryostat could be operated through several hours in the range 0.5 to 1.5 K by mere adjustment of the pumping rate. Temperature stability obtained this way ($\sim 10^{-3}$ K) was quite sufficient for our needs.

Measurement of the temperature can proceed in any of the following ways: Allen-Bradley carbon thermometer, ^{3}He saturated vapor pressure, or low-bias conductance of the aluminum diode. The thermal quasiparticle current of the latter was indeed found to obey the expected exponential dependence upon T^{-1} (see Sec. V), down to the lowest attainable temperature (0.47 K). As a result, when calibrated against the ^{3}He vapor pressure versus T curve, this provides a reliable thermometer in intimate contact with the sample itself.

The whole cryostat was shielded against earth and stray magnetic fields by a μ-metal enclosure, while an internal superconducting coil could be used to apply moderate fields (~ 1 kOe) parallel to the superconducting junctions.

The STJ constant current bias was supplied by a high-stability dc source.[18] On the other hand, accurate transit times of the phonon bursts were measured using a quartz-controlled delay generator (Applications des Techniques Nouvelles en Electronique, Orsay). Thanks to a very low-noise (~ 5 μV) first-

stage preamplifier,[19] phonon STJ signals as low as $\sim 0.1\ \mu$V (minimum) could be amplified and averaged in a PAR 160 Boxcar Integrator.

In fact, rather large signals were obtained at low temperature at the Al STJ with only a few 10^{-2} W of incident power, dissipated on an effective area (light spot) of about 0.02 mm^2. This is enough[20] to reach the heater temperature $T_H \gtrsim 3$ K, sufficiently above T according to the discussion of Eq. (7) while, at the same time, the STJ receiver remains within the linear range of detection.[1] Much higher powers (> 1 W) were required when using tin STJ as detectors. The reason is that, in this case, only a very small fraction of the heat-pulse spectrum is available for detection. To obtain such high powers, Joule emission, in spite of its inherent defect—electromagnetic ringing—had to be chosen in place of laser excitation, while the emitter area was increased to keep approximately the same heat flux per unit area.

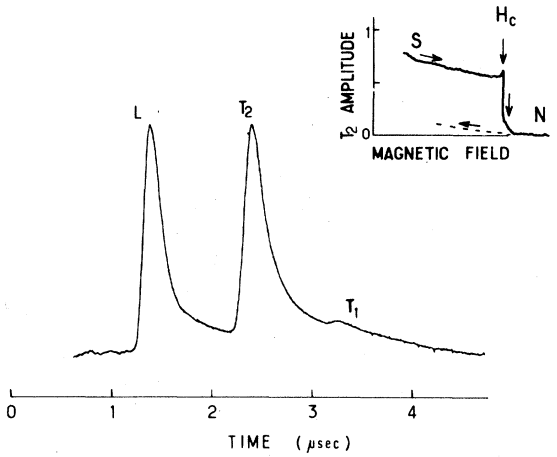

FIG. 5. Time-of-flight analysis of ballistic heat pulses along [110] in Sn. Superconducting Zn bolometer. Sample length: 4.0 mm. Temperature: 0.75 K. Inset shows the dependence of the T_2 signal amplitude vs magnetic field parallel to the surface (aluminum bolometer: 300 Å).

III. PHONONS WITHOUT INTERACTIONS

Below the critical temperature, subgap phonons ($h\nu < 2\Delta$) decouple from the electron system, as this is known from the T^3 behavior of the thermal conductivity, and ballistic propagation takes place.[8,9] The longitudinal (L) and transverse (T_1, T_2) acoustic branches give rise to time-resolved peaks (Fig. 5), which are identifiable by the corresponding velocities of sound. Indeed, heat-pulse transmission through superconducting tin shares much in common with that in a dielectric crystal.[16]

In contrast, the strong attenuation $\alpha_N = \Lambda_N^{-1} \gtrsim 10^4$ cm^{-1}, typical of the normal state, is readily restored by application of a magnetic field (inset of Fig. 5): as long as the field is lower than critical ($H_c = 260$ Oe in our geometry), the magnetic flux is expelled from the sample by Meissner effect; only the decrease of bolometer sensitivity is observed. At H_c, the whole phonon signal suddenly drops out. As the field is turned off, an important hysteretic effect is noted, which, however, may not be large on the scale of the sample size, since ballistic propagation can be perturbed by as thin as $\simeq 1$-μm-thick normal regions. Partial ballisticity is recovered in a few minutes, but

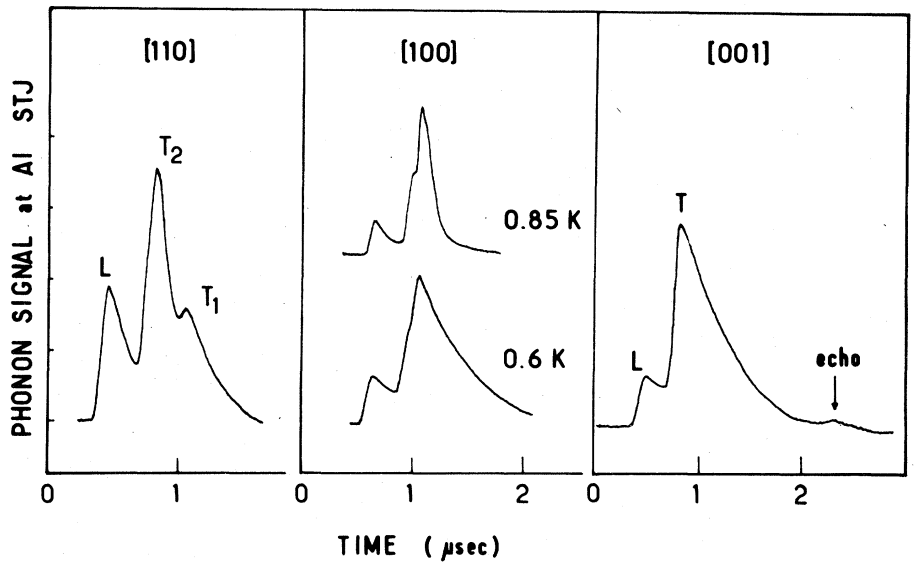

FIG. 6. Ballistic signals detected in tin crystals oriented along [110]: 1.0 mm; [100]: 1.62 mm; and [001]: 1.49 mm. Temperature is 0.6 K except when specified. Granular aluminum STJ detector.

complete expulsion of the flux can only be achieved through thermal cycling ($T > T_c$). It is worth noting, although no elementary explanation can be given at this stage, that, in the same conditions of input power and temperature as those of Fig. 5, there is no detectable heat-pulse signal in the normal state.[21]

Although acoustic properties of tin are rather well known, essentially from ultrasonic studies,[22] they are not easily accessible at thermal frequencies. Therefore, we devote the rest of this section to the information gathered from heat-pulse transmission.

As a member of the tetragonal holohedry, white tin is elastically characterized by a set of six second-order compliances[23] (see Appendix) or equivalently by an independent set of six sound velocities. The principal directions [100], [110], and [001] are the only ones to be associated with pure longitudinal and transverse polarizations. The corresponding heat-pulse signals versus time shown in Fig. 6 were taken at 0.6 K, a temperature low enough that attenuation by the thermal quasiparticles be negligible. Unfortunately, this low temperature is also responsible for the relatively slow response (typically 500 nsec) of the granular Al STJ. Upon raising the temperature, time resolution improves (at the expense of sensitivity) and some details, such as the composite structure of the transverse peak along [100], are revealed. We will come back to this point.

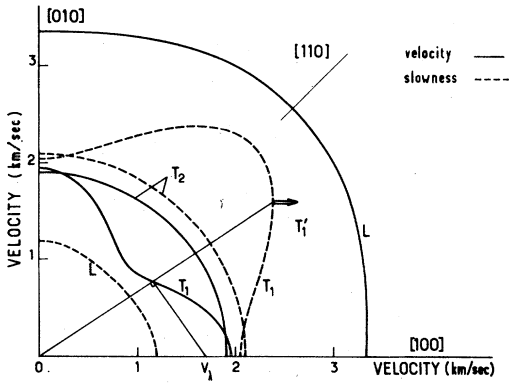

FIG. 7. Intersections of the velocity surface (——) and of the slowness surface (– – –) with the basal plane. Note the construction of the group velocity of the oblique mode T_1' propagating along [100].

Energy, or group, velocities $\vec{V}_\lambda$ (λ specifies the wave-vector direction and the polarization) are read directly from the heat-pulse transit times. Let us recall that, according to crystal acoustics, phase velocities $\vec{s}_\lambda$ and group velocities $\vec{V}_\lambda$ are not collinear in general; a given direction of energy flow may be in correspondence with several $\vec{q}$ vectors. As an illustration, let us consider the basal plane of the tetrago-

TABLE I. Acoustic parameters of heat-pulse propagation in white tin. Comparison with ultrasonic predictions (Ref. 22) (see text).

Direction of energy propagation	Mode[a]	Wave-vector direction[b]	Polarization	Group velocity[c] (km/sec)	Heat velocity (this work)	Relative mode intensities calculated[d]	this work
[100]	L	[100]	[100]	3.34	3.31	1	1
	T_1	[100]	[010]	1.95	2.02		
						3[e]	
	T_1'	$\theta = 90°$ $\phi = 33.65°$	$\theta = 90°$ $\phi = -52.42°$	1.68	1.78		3[f]
	T_2	[100]	[001]	1.91		1	
[110]	L	[110]	[110]	3.65	3.66	2	1
	T_1		[1$\bar{1}$0]	1.30	1.30	0	0.3
	T_2		[001]	1.91	1.94	1	1.6
[001]	L	[001]	[001]	3.74	3.8	1	1
	T_1, T_2	[001]	⟨001⟩ plane	1.91	2.0	4	5

[a]Notation of Ref. 24.
[b]Spherical coordinates. θ is the angle with the [001] axis, ϕ the azimuthal angle relative to the axis [100].
[c]Computed from the elastic constants of Ref. 22.
[d]Reference 24.
[e]Summation over modes T_1 and T_1' is understood.
[f]Summation over modes T_1, T_1', and T_2 is understood.

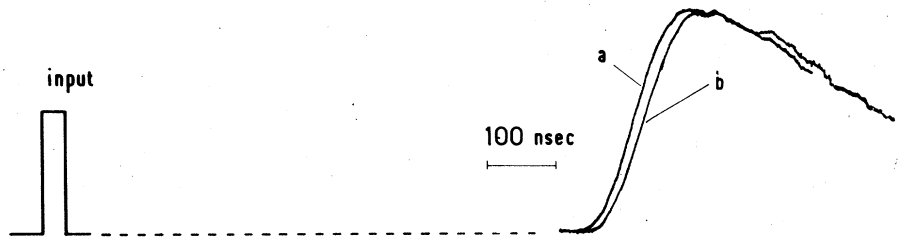

FIG. 8. Effect of velocity dispersion of the T phonons along [001]. Magnetically tuned STJ. (a) 210 Oe; (b) 160 Oe. Peak amplitudes are normalized for comparison. Temperature: 0.6 K.

nal lattice[23] and its intersections (Fig. 7) by the triple sheet of the slowness surface, defined as the locus of the extremity of the vector $(\vec{q}_\lambda/2\pi\nu_\lambda)$ and of the phase velocity $(\vec{s}_\lambda)$ surface, inverse of the preceding one. Energy velocity $\vec{V}_\lambda = 2\pi(\partial\nu_\lambda/\partial\vec{q}_\lambda)$ is normal to the slowness surface and verifies in absolute value

$$V_\lambda = s_\lambda/\cos(\vec{q}_\lambda, \vec{V}_\lambda) \quad . \tag{8}$$

Along [100] for instance, in addition to the three ordinary modes, there exists an off-axis mode, labeled T_1', 33.65° away from the [100] direction, with group velocity $V_\lambda = 1.68$ km/sec, computed from ultrasonic elastic constants.[22] More complete calculations concerning the tetragonal structure[24] show that T_1' is the only additional mode to have group velocity along [100]. It is responsible for the composite structure of the transverse peak at 0.85 K in Fig. 6, while the pure modes, having velocities 1.95 and 1.91 km/sec are not resolvable in time.

Elasticity is not the main purpose of this paper, so these problems will not be developed at length. We simply list in Table I the raw results of heat-pulse velocity measurements in front of the corresponding phase velocities taken from Ref. 22. The agreement is good enough in view of the uncertainties associated with both methods. The related subject of phonon focusing can also be approached in the same manner. For instance, the T_1 mode along [110], associated with a large curvature of the slowness surface will be a direction of defocusing (reduced energy transport). This is clear from Figs. 5 and 6, if one compares the T_1 and T_2 transverse peaks along [110]. Prediction of intensity ratios along a general direction requires extensive calculations.[24] Results for the symmetry directions, listed in Table I, show a relatively good agreement with the observations, especially if one considers all the imperfections from experimental origin (finite sample length, finite temperature and detector response time) or from the model (ignorance of the abundance of L and T modes in the sources, of the differential transmission factors at the interfaces, of modal dependence of the detectivity, etc.).

Chromatic dispersion[25] of the acoustical waves is often unduly overlooked in the context of heat pulses, while it provides a useful test of the high-frequency transmissivity of a given material. In view of the cutoff of ballistic transmission at $2\Delta/h \simeq 273$ GHz (in tin), dispersion of times of flights is not expected to reach large values. However, the effect is observable on transverse modes (Fig. 8): when the threshold of the Sn STJ detector is tuned by application of a magnetic field, transit times are reduced as less energetic (more rapid) phonons are detected.

Accuracy is not sufficient here to help in the determination of phonon dispersion relations. Nonetheless, it is a useful confirmation that one is indeed detecting high-frequency phonons.

IV. FREE PROPAGATION WINDOW: THE PAIR-BREAKING LIMIT

Among the various methods of determining the superconducting gap, the most direct one to date is that of tunnel conductance. It has produced most of the accepted values for metals and alloys. As regards the anisotropy of 2Δ, however, there remains a number of conflicting, or uncorrelated, results.[26] The ultrasonic (US) method, because it uses the bulk of the transmission medium, seems preferable: in this case, the gap is deduced from the quasiparticle population factor $\exp(-\Delta/k_B T)$, itself derived from the temperature dependence of the US attenuation. Our heat-pulse determination of 2Δ also uses a bulk effect, but differs from the US way in that the gap is resonantly probed by pair-breaking phonons $(h\nu \geq 2\Delta)$.

In effect, at low reduced temperatures, the attenuation of high-frequency phonons (see Fig. 1) exhibits the same accident as the density of electronic excitations, yielding mean free paths either much longer than the typical sample sizes ($\gtrsim 1$ mm) for subgap phonons, or considerably shorter for the pair-breaking phonons. The problem of determining 2Δ is that of finding the upper limit of the ballistic frequency window defined by Eq. (6). A tin STJ, finely tuned by a parallel magnetic field (H) is appropriate to perform a narrow-band analysis of that limit.

Propagation of phonons along [001] is an exemplary case. Along that direction, crystalline Sn is known[15] to possess a relatively small gap, below the

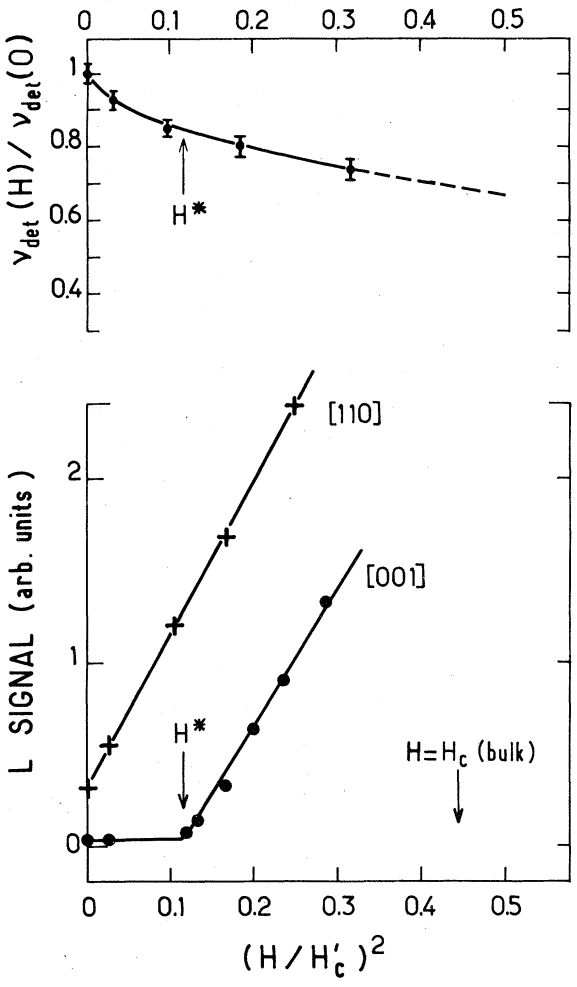

FIG. 9. Lower graph: plot of ballistic L signals along [001] and along [110] as a function of the squared reduced magnetic field (H/H_c'), where $H_c' \simeq 400$ Oe is the critical field of the tin STJ. Upper graph: chromatic-dispersion measurement (see text) of the threshold for detection, normalized in zero field. H^* is the kink value of the L signal along [001].

average gap typical of STJ films of the same material, so that the window is actually closed in zero field. Very faint signal amplitudes are indeed observed below the field $H^* = 135$ Oe. From there onward, and despite the (small) reduction of the STJ sensitivity, a steep rise of the L signal occurs (Fig. 9), giving evidence of the opening of the ballistic window. It must be noted that the property described above requires some directional definition: if the aperture angle of the phonon beam exceeds $\sim 30°$, as this was the case in Ref. 8, the T signal does not vanish in zero field. Clearly, this is associated with a larger gap for some phonons off axis from the [001] direction.

The gap of interest here is the minimum condensation energy of the pairs interacting with the chosen phonon mode. It can be identified to $h\nu_{det}(H^*)$ where H^* has the above meaning. Since, in a magnetic field, ν_{det} cannot be unambiguously extracted from the current-voltage characteristics of the STJ, we resort to the other determination based on chromatic dispersion of high-frequency phonons. We refer for description of the method to previous work performed on indium antimonide crystals[25]: in essence, it consists in measuring the time of flight of the ballistic signals and relating it to the acoustic dispersion curves; one thus obtains the minimum detected frequency ν_{det} from the measured group velocity. We emphasize that ν_{det} receives this way a sharp definition, even in a magnetic field. A weaker point is the assumption of reproductibility of the STJ when we apply this calibration to experiments on another substrate (similarity of two junctions is decided from their current versus voltage characteristics).

Calibration of $\nu_{det}(H)$, performed on an InSb transmission medium,[27] is reported in the upper part of Fig. 9, showing tunability of at least $\sim 30\%$ of the tin STJ threshold frequency. The latter is read as 230 GHz, or $3.0 k_B T_c$ for $H = H^*$. Along [110], since ballistic signals show up in zero field (Fig. 9), the bulk gap $2\Delta_{Sn}$ must be superior to the STJ threshold $h\nu_{det}(H=0)$. In such a case, its value is obtainable by extrapolation of the signal amplitude in frequency

TABLE II. Measurements of superconducting gaps (in units of $k_B T_c$) by hf phonons (this work) compared with ultrasonic data taken from Ref. 15 for L modes, and Ref. 11 for T modes.

$\vec{q}$ direction	[100]	[100]	[100]	[110]	[110]	[110]	[001]	[001]
Polarization	L[100]	T_1[010]	T_2[001]	L[110]	$T_1[1\bar{1}0]$	T_2[001]	L[001]	T(basal plane)
hf phonons				3.7±0.15	3.7±0.2	3.7±0.15	3.0±0.1	3.0±0.1
US data	3.55±0.04	3.7±0.2	3.3±0.2	3.84±0.07			3.15±0.04	3.4±0.2

space rather than in magnetic field space.[8] Crystalline gaps measured by our method ("high-frequency or hf phonons") are compared in Table II with data deduced from the temperature dependence of ultrasonic attenuation.

We have not been able to detect any difference between the gaps measured with L and T waves belonging to the same wave vector, contrary to what happens along [001] for US waves. Otherwise, hf phonons yield results in agreement with US data, except for T phonons along [001] for which, in our opinion, the respective accuracies are such that one can conclude to a significant difference. The US method, except at very low temperature, gives an average over an effective zone, after Eq. (5), while the hf method involves a resonant process which will sample *minimum* values on the same zone. This is the most plausible explanation in view of the fact that our q values ($\simeq 10^7$ cm^{-1}) are still too small to reach the umklapp processes (if this was so, L and T phonons would likely be associated with different energy gaps).

One may add two remarks to this section: (i) there is no indication of any "smearing out" of the pair-breaking threshold and (ii) by low-pass filtering in the transmission medium and quantum detection in the STJ, one selects a rather narrow frequency window out of the initial heat pulse (270 to 285 GHz at $H=0$ for phonons having $\vec{q}$ // [110], for instance).

V. CALIBRATION OF Al STJ AND MEAN-FREE-PATH MEASUREMENTS

Generally speaking, phonon damping in the superconductor is the superposition of the electron-phonon scattering, with coefficient $\alpha_S=\alpha_{QP}+\alpha_{PB}$ from Eq. (3), and of other processes, such as defect and phonon-phonon scatterings, which we combine into a single coefficient α'. Let $G_\lambda(\nu)$ be the broadband spectrum (phonon number density in frequency space) generated at the emitter in the mode λ, and $S(\nu)$ be the STJ sensitivity, that is the voltage developed, in constant current bias conditions, by the STJ subjected to unit phonon flux. For a propagation length d, one collects in the steady-state regime, signals whose amplitude δV_λ is proportional to:

$$\delta V_\lambda \sim \int_0^\infty d\nu\, G_\lambda(\nu) S(\nu) \exp[-(\alpha_{QP}+\alpha_{PB}+\alpha')d] \quad . \tag{9}$$

All functions under the integration sign are virtually frequency and temperature dependent. However, the complexity of Eq. (9) is only apparent. Zero transmissivity of tin above the pair-breaking limit $h\nu=2\Delta_{Sn}$, and zero detectivity of the STJ (granular aluminum) below the threshold $h\nu_{det}=2\Delta_{Al}$ permit to sort out of the initial spectrum the restricted interval (see Fig. 3): $2\Delta_{Al}\leqslant h\nu<2\Delta_{Sn}$. This integration domain in turn may be considered as independent of the temperature, provided T is kept low enough compared to the critical temperatures of both tin and granular Al. Same thing can be said about the emission spectrum $G_\lambda(\nu)$ itself (see Sec. II for a discussion of this point). As to α', we merely assume it to be negligible or, at least, temperature independent, on account of the ballisticity observed (Figs. 5 and 6) when no electron-phonon interactions are present.

If one writes explicitly all temperature dependences, one has

$$\delta V_\lambda(T) \sim \int_{2\Delta_{Al}}^{2\Delta_{Sn}} d(h\nu)\, G_\lambda(\nu) S(\nu,T) \times \exp[-\alpha_{QP}(\nu,T)d] \quad . \tag{10}$$

While the T dependence of S can by no means be ignored, our aim is to disclose that of α_{QP}. This is possible thanks to the bulk size of d, which acts as an enhancement factor for the variations of α_{QP} and makes the temperature variations of $S(\nu,T)$ become secondary. In addition, the STJ detectivity can be handled by independent means and we now devote to this question a detailed discussion.

In a first step, we recall some basic features[1] of phonon detection in the (unrealistic here) limit of pulse durations δt long compared to the STJ response time τ_{eff} (STJ under steady phonon irradiation). Let δN be the incremental quasiparticle density inside the electrodes induced by the flux $\dot{n}_{ph}$ of $h\nu\geqslant 2\Delta_{Al}$ phonons. We assume δN to be much smaller than N_b, the quiescent density at bias current I_b (corresponding voltage is named V_b). In this small signal regime, the voltage drop δV across the junction follows a proportionality law:

$$\delta V \sim -R_b(T)\delta N \tag{11}$$

in which $R_b(T)=(dV/dI)_T$ is the dynamic resistance of the junction measured at V_b along the isotherm T, and with other proportionality factors nondependent upon the temperature. Therefore, because of the relation

$$\delta N \sim 2K\dot{n}_{ph}\tau_{eff}(T) \tag{12}$$

between δN and the response time τ_{eff} (K being the probability for an incident phonon to be absorbed in the film), the T dependence of the sensitivity goes essentially as that of τ_{eff}. The latter is itself closely related, through the "phonon trapping factor" introduced by Rothwarf and Taylor,[28] to the inverse density of quasiparticles present in the film. In the low-temperature approximation, one has[1]

$$N=N_{th}(T) = 2N(0)(2\pi\Delta_{Al}k_BT)^{1/2}\exp(-\Delta_{Al}/k_BT) \tag{13}$$

(the index th denoting thermal equilibrium values), and τ_{eff} should nearly fit the exponential law in T^{-1}

$$\tau_{\text{eff}} = \tau_{\text{th}}(T) \simeq \tau_0 \exp(\Delta_{\text{Al}}/k_B T) \tag{14}$$

if one forgets the $T^{-1/2}$ dependence. In the above equations, we have used $N(0)$ to be the single-spin density of electronic states at the Fermi level in Al, and τ_0 a time constant depending upon the STJ constitution parameters. However, Eqs. (13) and (14) no more hold valid in the over-injection case, $N_b > N_{\text{th}}$, corresponding to bias currents larger than the thermal current I_{th} (I_{th} is taken on the plateau of the I-V curves preceding $V = \Delta_{\text{Al}}/e$). Then, if $\dot{N}_>$ is the quasiparticle population injected per unit time, per unit volume of the junction, by the over-injection current defined as $I_b - I_{\text{th}}$, one has[28]

$$\tau_{\text{eff}}^{-2} = \tau_{\text{th}}^{-2} + 2\tau_{\text{th}}^{-1}\, \dot{N}_>/N_{\text{th}} \ . \tag{15}$$

The suitability of superconducting junctions can be checked in several ways. The current-voltage isotherms of Fig. 10 show a very large midgap structure starting at $V_b \simeq 0.31$ mV, which may be attributed either to two-particle tunneling,[29] or to other nonideal processes likely to generate subharmonics. Below this step, and down to the lowest accessible temperature, the "thermal" current measured on the plateau (at $V_b = 0.25$ mV) is found to obey the exponential law

$$I_{\text{th}} = I_0 \exp(-\Delta_{\text{Al}}/k_B T) \ , \tag{16}$$

with $I_0 = 11.3$ mA and $2\Delta_{\text{Al}} = 0.625$ meV measured on the I-V curve.

The time τ_{eff} estimated from the decay of the response to a δ excitation (laser pulse of duration $\simeq 20$ nsec) is also found to follow an exponential law (14), with $\tau_0 = 1.35$ nsec at $V_b = 0.25$ mV (measurements extend from 2200 nsec at 0.47 K down to $\lesssim 50$ nsec at 1.10 K).

One avoids this inconvenient variation of the response time, and of the sensitivity through Eqs. (11) and (12), by working in the over-injection region ($\Delta_{\text{Al}} < eV_b < 2\Delta_{\text{Al}}$). In this region, the recombination rate of the quasiparticles is determined, not by the strongly T-dependent N_{th} population, but rather by the nonequilibrium population imposed by the over-injection current already defined in connection with Eq. (15). Indeed, the inverse squared response times measured at 0.47 K verify[30] quite satisfactorily

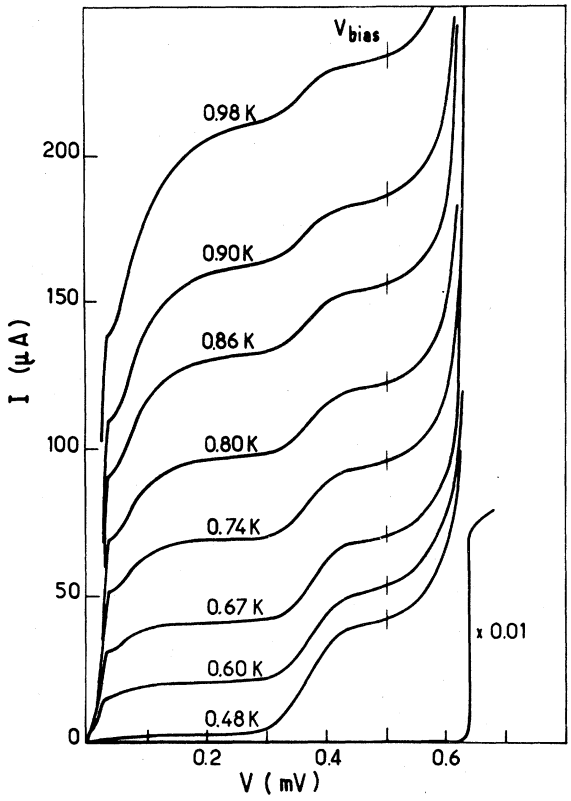

FIG. 10. Current vs voltage isotherms of a granular aluminum STJ. Note the large midgap structure. Parallel field: 50 Oe. For phonon detection, the bias was fixed at $V = 0.5$ mV, where the dynamic resistance is practically T independent.

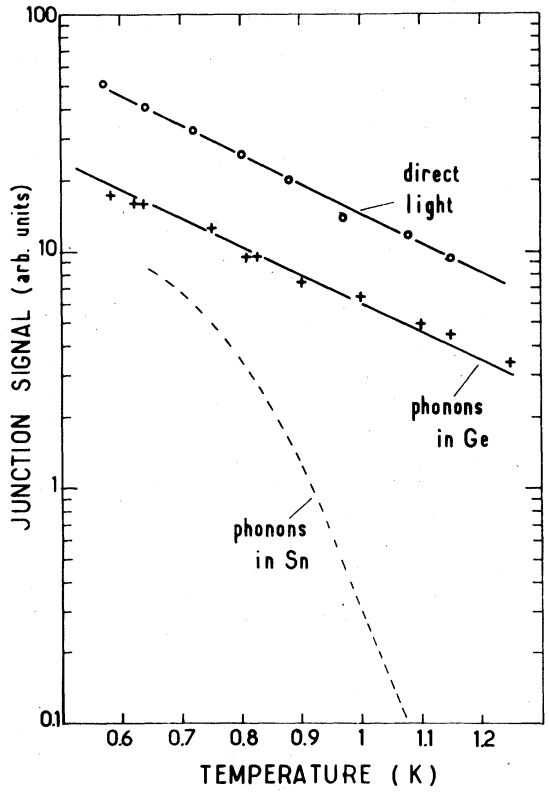

FIG. 11. Calibration of the granular Al STJ by laser pulses (○) and by a reference phonon pulse in a dielectric (+). Dotted line shows a typical plot of a heat-pulse signal in Sn (L mode along [100]).

the expected linear dependence upon $\dot{N}_>$, up to the point that it becomes possible to deduce $N(0)$ from Eqs. (13) and (15). We obtain in this manner $N(0) = (1.65 \pm 0.20) \times 10^{22}$ eV^{-1} cm^{-1}, in perfect agreement with the values[31] found for pure Al and for granular Al having a $T_c = 1.85$ K lower than ours ($T_c = 2.05$ K). That seems to confirm that the explanation for the enhancement of T_c is not to be looked for in the variations of $N(0)$.

Sensitivity to an energy flux was calibrated in the following way. The STJ under study was irradiated *in situ* (Fig. 4) by a laser pulse adjusted in amplitude and duration (160 nsec) so as to give at the STJ signals comparable to the phonon small signals that are detected. T dependence of such a reference pulse (at fixed laser intensity) is plotted in Fig. 11. It shows a decrease by a factor 5 of the sensitivity between 0.6 and 1.2 K. Fortunately, that is still small compared to the variation, by a factor > 100, of a ballistic phonon pulse (L mode along [100]) having traveled in a 1.62-mm-thick Sn sample. Let us again remark that the stabilization of the STJ sensitivity, without which no attenuation measurement could have been performed in confidence, is a result of over injection.

A second calibration procedure, which can alternatively be considered as a test of the first one, uses the—temperature independent, in principle—phonon propagation in a dielectric crystal. We excite, by conventional Joule effect, heat pulses in a pure germanium sample with an input power of 10 W/cm^2, giving rise to a heater temperature $T_H \simeq 3$ K according to the analysis of Sec. II. In such conditions, with little doubt one can admit (i) that the generated frequency spectrum $G_\lambda(\nu, T)$ is practically independent of the substrate temperature T from 0.6 to 1.2 K and (ii) that phonon attenuation in Ge is negligible in the same range. As noted in Fig. 11, there is a strict proportionality between the detected heat pulses in Ge and the calibrating laser pulses detected at the same T.

VI. DISCUSSION OF RESULTS

Putting $A_\lambda = \delta V_\lambda / \delta V_{\text{cal}}$, where δV_{cal} is the laser calibration signal, defines a transmission factor up to an additive constant. The latter is fixed on taking as unit of A_λ its low-temperature "plateau" value A_λ^0, that corresponds to vanishing of the bulk attenuation ($\alpha_{\text{QP}} \simeq 0$). So, one introduces the transmission coefficient, in decibels per centimeter, directly proportional to the attenuation (in cm^{-1})

$$(10/d)\log_{10}(A_\lambda / A_\lambda^0) = -4.34\alpha_{\text{QP}} \ . \qquad (17)$$

A plot of the above quantity against temperature is shown in Fig. 12 for the longitudinal mode along [100]. Compatibility of the measurements for several sample lengths had already been checked for the

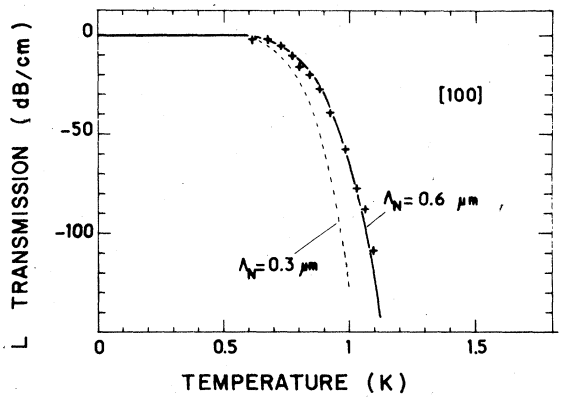

FIG. 12. Plot of the transmissivity, as defined by Eq. (17), of $\nu \geq 150$ GHz longitudinal phonons along [100] as a function of the temperature. Theoretical fit (bold line) uses $2\Delta = 3.52 k_B T_c$ and $\Lambda_N = 0.6$ μm. Dashed line corresponds to $\Lambda_N = 0.3$ μm.

[110] direction.[8] From experiment, it appears that L attenuation is dependent upon the wave-vector direction, being strongest along [100] at a given temperature. Dependence upon the polarization (not shown) does not obey a general rule: along [110], T_1, then T_2 modes vanish with increasing temperature before L does (see Fig. 1 of Ref. 8). On the contrary, $\alpha_{\text{QP}}(T) < \alpha_{\text{QP}}(L)$ for phonons propagating along [100].

Our conclusions are obviously relevant not to monochromatic phonons, but to the integration band of Eqs. (6) and (10). However, upon consideration that (a) the STJ sensitivity is peaked at the threshold of detection and (b) transmissivity is a decreasing function of ν ($\Lambda_N \sim \nu^{-1}$), it is reasonable to refer to the single frequency: $\nu = \nu_{\text{det}} \simeq 150$ GHz.

Numerical fit to the experiments proceeds from Eq. (3b) where, among the parameters Δ and $\alpha_N = \Lambda_N^{-1}$, only the second one remains unknown. Since we are now considering the attenuation of subgap phonons, the "EZ-averaged" gap resulting from US data look better suited than our Δ values corresponding to the threshold of pair breaking (Sec. IV). With this choice of Δ, Λ_N is then adjusted to yield a best fit such as that of Fig. 12 which was obtained with $2\Delta = 3.52 k_B T_c$ and $\Lambda_N = 0.6$ μm for the L mode along [100]. Experimental accuracy has been much improved upon Ref. 8, thanks to laser calibration, to such extent that the choice of Δ, not the scatter of experimental data, becomes the major source of uncertainty. In fact, Λ_N turns out to be rather sensitive upon Δ: a reduction of Δ by 2% causes an increase of about 10% in Λ_N. Therefore, our Λ_N cannot be credited better than 20% accuracy.

Table III contains for each principal mode the normal mean free paths thus obtained and the coupling constant $C(\vec{q}, \vec{e}_q)$ related to it via Eq. (2) (phonon

TABLE III. Electron-phonon coupling parameters in tin deduced from mean-free-path measurements at $\nu \gtrsim 150$ GHz.

Propagation direction	[100]	[100]	[100]	[110]	[110]	[110]	[001]	[001]
Polarization	L [100]	T_1 [010]	T_2 [001]	L [110]	T_1 [1$\bar{1}$0]	T_2 [001]	L [001]	T (basal plane)
$2\Delta/k_B T_c$[a]	3.52	3.52	3.52	3.88	3.88	3.88	3.20	3.20
$\Lambda_N(\mu m)$	0.6	1.5[b]	1.5[b]	1.2	0.4	0.7	2	2
C (eV) (this work)	6.9	2.5[b]	2.5[b]	5.5	3.4	3.8	4.3	2
C (eV) from US data[c]	6.3	2.2	1.3	5.7	~ 0.7		6.1	2.4
τ_{PB} (psec)	60	270	110	105	125		180	360

[a]Value selected for theoretical fit.
[b]Averaged over modes T_1, T_1', and T_2'.
[c]Derived from the normal attenuation constant given in Ref. 11: α_N for L modes and α_{def} for T modes (see text).

frequency assumed to be 150 GHz). C is a convenient parameter to express the strength of the electron-phonon interaction in a frequency-independent way. C can also be derived from Leibowitz's work[11] on 30-MHz ultrasonic attenuation: for L waves, one straightforwardly applies Eq. (2) at the relevant frequency. For T waves, on the contrary, the US attenuation is a combination of several mechanisms

$$\alpha_N = \alpha_{em} + \alpha_{cd} + \alpha_{def} \tag{18}$$

out of which only the latter has the character of a "deformation potential" interaction and gives a contribution to C. The electromagnetic attenuation α_{em} vanishes in the superconducting state and, so, can be subtracted as soon as the discontinuous drop of α_S just below T_c is known.[11] The collision drag term α_{cd}, inversely proportional to ql, also vanishes in the hf range; it is estimated through its relationship with the $g(ql)$ Pippard function.[12] This procedure leaves about 40% of the total transverse attenuation at 30 MHz to α_{def}, which turns out to be the only contribution to C in the hf range, unless umklapp processes arise for large wave vectors, that would have been inoperant in US observations.

Between US and hf (this work) deformation potentials C, the agreement is surprising in view of the difference of the experimental conditions and the scale of extrapolation (four orders of magnitude). This is without contest a success of the theoretical treatment of electron-phonon interaction. As a consequence, it seems unnecessary to introduce the umklapp processes that have been invoked[6,7] to explain thin-film results. An exception might be made for the T_1 mode along [110] which corresponds to relatively large wave vectors ($\sim 10^7$ cm^{-1}) and for which the discrepancy between the two values of C is largest (unfortunately, for this mode, α_{def} is only 10% of the total US attenuation, so the accuracy of C deduced from US data is probably poor).

Pair-breaking lifetimes τ_{PB}, or lifetimes of $h\nu \geqslant 2\Delta$ phonons, are also important parameters in problems involving the "phonon-trapping factor."[1,2] If one postulates electron-phonon coupling is regular through the gap energy, one can make a smooth extrapolation of $|g(q)|^2 \sim \nu$ up to the gap frequency to get

$$\tau_{PB}^{-1} = \tfrac{1}{2}\pi \frac{2\Delta}{h\nu_{det}} \frac{V_\lambda}{\Lambda_N(\nu_{det})} , \tag{19}$$

where Δ, V_λ, and Λ_N are, respectively, the half-gap, group velocity, and normal mean free path of the mode (λ) one considers. These τ_{PB} are reported in Table III. A comparison is possible with the 110 psec derived[32] from inelastic tunnel conductance (the notation for τ_{PB} is τ_0^{ph} in the referenced work by Kaplan *et al.*).

To permit a prediction useful in the context of thin-film absorption and so-called phonon fluorescence, it is also possible to perform an average of the pair-breaking mean free paths over the principal modes

$$(\bar{\Lambda}_{PB})^{-1} = \langle 1/V_\lambda \tau_{PB} \rangle_\lambda . \tag{20}$$

In this equation, the bracket $\langle\ \rangle_\lambda$ indicates averaging over the principal modes with the weighting factor s_λ^{-2} to account for the phonon density of states in each acoustic branch (this puts emphasis on the transverse modes). One thus finds: $\bar{\Lambda}_{PB} \simeq 2700 \pm 500$ Å.

Much lower values were deduced either from fluorescence efficiency[6] ($\bar{\Lambda}_{PB} \lesssim 600$ Å), or from reabsorption of recombination phonons in a STJ[7] ($\bar{\Lambda}_{PB} \lesssim 1000$ Å). In contrast, the escape of greater

TABLE IV. Eigenvalues ρs_λ^2 of matrix (A2) for the principal directions.

Polarization \ Wave vector	[100]	[110]	[001]
L	c_{11}	$1/2(c_{11}+c_{12}+2c_{66})$	c_{33}
T_1	c_{66}	c_{44}	c_{44}
T_2	c_{44}	$1/2(c_{11}-c_{12})$	c_{44}

than 2Δ phonons from 0.3–0.7-μm Sn films,[33] or the incomplete filtering in 4000-Å-thick films[34] are compatible with pair-breaking mean free paths of several thousand angstroms. In our opinion, the interface conditions (towards substrate or helium bath), and possible participation of quasiparticles in the transport of excitations,[33] contain enough uncertainty to explain the discrepancies of thin-film estimations.

To summarize, no supplementary (umklapp) process affects sensibly the lifetimes of near-gap phonons. Measured mean free paths are indeed in surprising agreement with the extrapolated ultrasonic data. It is also amusing to note that the electron-phonon coupling constants associated to L modes approach the free-electron value, i.e., $\frac{2}{3}$ times the Fermi energy ($\simeq 10.3$ eV in tin). On the other hand, ballistic propagation suggests a lifetime against phonon-phonon decay $\gtrsim 1$ msec around 1 K.

ACKNOWLEDGMENTS

The authors are indebted to N. Lockerbie and D. Huet for valuable contribution and to Professor J. Bok for his interest in the work.

APPENDIX: ELASTIC WAVES IN THE TETRAGONAL STRUCTURE

The general equation defining the normal modes in an anisotropic medium of mass density ρ ($\rho = 7.387$ g cm^{-3} for tin at 4.2 K) reads

$$c_{ijkl} n_k n_l u_i = \rho s_\lambda^2 u_j \ . \tag{A1}$$

In this equation, a mode (λ) is defined by its polarization vector u_i and its direction cosines of wave vector n_i. The elasticity tensor c_{ijkl} for the tetragonal structure depends upon six independent elastic constants, labeled c_{11}, c_{12}, c_{13}, c_{22}, c_{44}, and c_{66} in the usual notation.[23] From Eq. (A1), $\{u_i\}$ and ρs_λ^2 are, respectively, the eigenvectors and the eigenvalues of the matrix

$$\begin{pmatrix} c_{11}n_x^2 + c_{66}n_y^2 + c_{44}n_z^2 & (c_{12}+c_{66})n_x n_y & (c_{13}+c_{44})n_x n_z \\ (c_{12}+c_{66})n_x n_y & c_{66}n_x^2 + c_{11}n_y^2 + c_{44}n_z^2 & (c_{13}+c_{44})n_y n_z \\ (c_{13}+c_{44})n_x n_z & (c_{13}+c_{44})n_y n_z & c_{44}(n_x^2+n_y^2) + c_{33}n_z^2 \end{pmatrix} \ . \tag{A2}$$

In the basal plane ($n_z = 0$), of particular interest here, the characteristic equation for the T_2 modes (polarization along [001]) is $\rho s_\lambda^2 - c_{44} = 0$, which factorizes out of the general secular equation. The two other modes L and T_1 have both their wave vector and polarization vector in the basal plane.

Phase velocities of pure modes can be deduced from Table IV.

*Laboratoire associé au Centre National de la Recherche Scientifique et Université Paris VII.

[1]W. Eisenmenger, in *Physical Acoustics*, edited by W. P. Mason and R. Thurston (Academic, New York, 1976), Vol. XII.

[2]D. N. Langenberg, in *Proceedings of the Fourth International Conference on Low Temperature Physics*, edited by M. Krusius and M. Vuorio (North-Holland, Amsterdam, 1975).

[3]W. L. McMillan and J. M. Rowell, in *Superconductivity*, edited by R. D. Parks (Marcel Dekker, New York, 1969), Vol. 1.

[4]S. M. Shapiro, G. Shirane, and J. D. Axe, Phys. Rev. B 12, 4899 (1975).

[5]A. R. Long, J. Phys. F 3, 2023 (1973).

[6]R. C. Dynes and V. Narayanamurti, Phys. Rev. B 6, 143 (1972).

[7]W. Eisenmenger, K. Lassmann, H. J. Trumpp, and R. Krauss, Appl. Phys. 12, 163 (1977).

[8]B. Pannetier, D. Huet, J. Buechner, and J. P. Maneval, Phys. Rev. Lett. 39, 646 (1977).

[9]V. Narayanamurti, R. C. Dynes, P. Hu, H. Smith, and W.

F. Brinkman, Phys. Rev. B 18, 6041 (1978).
[10]A. H. Wilson, *The Theory of Metals* (Cambridge University Press, Cambridge, England, 1953).
[11]J. R. Leibowitz, Phys. Rev. 133, A84 (1964); 136, A22 (1964).
[12]A. B. Pippard, Proc. R. Soc. London Ser. A 257, 165 (1960).
[13]J. Bardeen, G. R. Rickayzen, and L. Tewordt, Phys. Rev. 113, 982 (1959).
[14]A. P. Cracknell and K. C. Wong, *The Fermi Surface* (Clarendon, Oxford, 1973).
[15]J. M. Perz and E. R. Dobbs, Proc. R. Soc. London Ser. A 297, 408 (1967).
[16]D. Huet, B. Pannetier, F. R. Ladan, and J. P. Maneval, J. Phys. (Paris) 37, 521 (1976). This reference contains a more complete description of the heat-pulse method.
[17]O. Weis, J. Phys. (Paris) 33, C4-49 (1972).
[18]B. L. Blackford, Rev. Sci. Instrum. 42, 1198 (1971). Our instrument is a modified version of the voltage source described in this reference.
[19]We thank H. Kinder for information about this point.
[20]The blackbody-radiation model with perfect match provides an upper limit for σ. According to Ref. 17, $\sigma = 0.11$ W cm^{-2} K^{-4} for copper.
[21]Contrary to the simple-minded expectation that heat conductivity is larger in the normal state, at least in near-equilibrium conditions.
[22]J. A. Rayne and B. S. Chandrasekhar, Phys. Rev. 120, 1658 (1960).
[23]M. J. P. Musgrave, in *Crystal Acoustics,* edited by J. J. Brandstatter (Holden-Day, San Francisco, 1970).
[24]C. G. Winterheimer and A. K. McCurdy, Phys. Rev. B 18, 6576 (1978).
[25]D. Huet, B. Pannetier, and J. P. Maneval, in *Phonon Scattering in Solids,* edited by L. J. Challis, V. W. Rampton, and A. F. G. Wyatt (Plenum, New York, 1976), p. 283. See also D. Huet, J. P. Maneval, and A. Zylbersztejn, Phys. Rev. Lett. 29, 1092 (1972).
[26]J. L. Bostock and M. L. A. Mac Vicar, in *Anisotropy Effects in Superconductors,* edited by Harold W. Weber (Plenum, New York, 1977).
[27]D. Huet, Ph.D. thesis (Université Pierre et Marie Curie, Paris, 1978) (unpublished).
[28]A. Rothwarf and B. N. Taylor, Phys. Rev. Lett. 19, 27 (1967).
[29]W. Forkel and H. Schenk, J. Phys. (Paris) 39, C6-593 (1978).
[30]B. Pannetier, Ph.D. thesis (Université Pierre et Marie Curie, Paris, 1980) (unpublished).
[31]P. W. Epperlein and W. Eisenmenger, Z. Phys. B 32, 167 (1979).
[32]S. B. Kaplan, C. C. Chi, D. N. Langenberg, J. J. Chang, S. Jafarey, and D. J. Scalapino, Phys. Rev. B 14, 4854 (1976).
[33]J. L. Singer and W. E. Bron, Phys. Rev. B 14, 2832 (1976).
[34]D. Huet, B. Pannetier, and F. R. Ladan, *Internal Friction and Ultrasonic Attenuation in Solids* (University of Tokyo, Tokyo, 1977), p. 151.